A Mass Conservative Lattice Boltzmann Model for Two-phase Flows with Moving Contact Lines at High Density Ratio

Tao Lu,[1] Xuguang Yang,[2, 3] Fu Xiao[1,*] and Tao Wen[1]

[1]Department of Building Services Engineering, The Hong Kong Polytechnic University, Hong Kong, China

[2]Department of Applied Mathematics, The Hong Kong Polytechnic University, Hong Kong, China

[3]School of Mathematics and Computational Science, Hunan First Normal University, Changsha, China

[*]Corresponding author: linda.xiao@polyu.edu.hk

ABSTRACT

In this paper, a mass conservative lattice Boltzmann model (LBM) is proposed to simulate the two-phase flows with moving contact lines at high density ratio. The proposed model consists of a phase field lattice Boltzmann equation (LBE) for solving the conservative Allen-Cahn (A-C) equation, and a pressure evolution LBE for solving the incompressible Navier-Stokes equations. In addition, a modified wall boundary treatment scheme is developed to ensure the mass conservation. The wetting dynamics are treated by incorporating the cubic wall energy in the expression of the total free energy. The current model is characterized by mass conservation, proper treatment of wetting boundary and high density ratio. We applied the model on a series of numerical tests including equilibrium droplets on wetting surface, co-current flow and a droplet moving by gravity along inclined wetting surfaces. Theoretical analysis and experiments are conducted for model validation. The numerical results show good performances on mass conservation even with a density contrast up to 1000. Furthermore, the results show that the moving contact line can be successfully recovered, which proves that this model is applicable on the study of moving contact line issue and further related applications.

Keywords

Lattice Boltzmann model, Two-phase flow, Moving contact line, High density ratio

1. INTRODUCTION

The behavior of droplets on wetting surfaces is always a popular research topic because it is the multiphase flow fundamental of many engineering applications. The contact angle, which is defined as the angle between the contact line and the solid surface, is an important parameter characterizing the wettability, which significantly influence the behavior of droplets on wetting surfaces. If the solid surface is not horizontal and the gravity exists, the droplet may move on the surface and so as the triple contact line. In this situation, the moving contact line is observed and dynamic contact angles should be defined to feature this phenomenon. The study of the moving contact line is of great significance in engineering applications such like chip cooling, painting, coating and falling film based liquid desiccant technology [1,2]. The mechanism of formation of contact line has been studied theoretically by many researchers [3,4] and it is possible to predict the final equilibrium state of contact lines. However, the transition process, which is important for understanding the mechanism of moving contact line phenomenon, has not been sufficiently understood in previous theoretical studies. Considering the difficulties in conducting experimental study, numerical methods are more competent for studying the moving contact line.

The lattice Boltzmann method (LBM), which is a numerical method rooted in kinetic theory, is becoming popular in the fields of computational fluid dynamics in last decades [5-7]. Due to the particle-based mesoscopic nature which connects the micro and macro worlds, the LBM has an advantage in simulation fidelity and computational efficiency especially for multiphase flows [8,9]. A number of LB models for multiphase flows have been developed in previous researches [10], such as color-gradient model [11], Shan-Chen model [12,13], free energy model [14,15] and phase-field model [16,17]. An extended Shan-Chen method, in which the equation of state (EOS) and surface tension can be tuned independently, was developed by Sbragaglia et al to analyze the physical behavior of a class of mesoscopic models for multiphase flows[18]. Colosqui presented a dynamic optimization strategy to generate customized equations of state for the numerical simulation of non-ideal fluids at high density ratio [19]. The phase-field LB model, which is originally developed by He et al. [16] in 1998, has been proved applicable to high density ratio issue, which is a key challenge in modelling moving contact angle. Two distribution functions are taken in this model, one is for describing the fluid dynamics and the other is used to track the phase interface, and two macroscopic equations can be recovered from the distribution functions. The combination of Navier–Stokes (N-S) and Cahn-Hilliard (C-H) equation is applied in many phase field LBMs. Lee and Liu [20] successfully simulate the contact angle at high density ratio with a proposed C-H based LBM. Liang et al [21] reported their C-H based LBM can properly describe the axisymmetric multiphase flows. However, due to the simplification made in the recovering process, the C-H based phase field LBMs cannot

ensure mass conservation. Around 1% of mass change ratio was observed in Connington and Lee's work [22]. Although the error is not large, it may be unacceptable in some special applications. For example, Zheng et al [23] reported that in their modelling, the small droplets disappeared if their radius was below a critical value. A conservative LBM for interface tracking was proposed by Fakhari et al [24] in 2016. The model was also based on the phase field theory, but it recovered the Allen-Cahn (A-C) equation instead of the Cahn-Hilliard equation, while the former is conservative. Due to its advantages in mass conservation, the A-C based LBM is becoming more popular. The newly developed model by Fakhari et al [24] has shown great advantage in terms of mass conservation, speed-up and efficiency compared to the Lee and Liu's C-H based model [20] on the contact angle simulation. Liang et al [25] investigated the droplet impact on a thin liquid film with a large density ratio of 1000 and successfully reproduced the droplet splashing phenomenon with a A-C based LB model. However, many A-C based LBMs are proposed for the equilibrium problems, whether the method can be applied on the moving contact line is still unknown.

Another big challenge in moving contact line simulation by LBM is the treatment of wetting boundary. Yan and Zu [26] developed a LB model for simulate the liquid droplet behavior on partial wetting surfaces with density ratio with a simple bounce back boundary scheme applied. While the results of their simulations agreed well with the theoretical prediction in equilibrium situations, the comparison of transient profiles between simulation and theory or experiments was not reported. Mazloomi et al applied the entropic lattice Boltzmann stabilization mechanism to control the dynamics at the liquid-vapor interface and developed a novel entropic lattice Boltzmann model (ELBM) for multiphase flows [27]. The model is used to investigate the dynamics of the contact line in a wide range of applications, from capillary filling to liquid drop impact onto a flat surfaces with different wettability [28]. They further extended the model to simulate large Weber and Reynolds number collisions of two droplets with a novel polynomial equation of state [29]. Accurate three-dimensional simulations involving realistic macro-textured surfaces were performed based on the ELBM [30] . Liu and Lee assumed that the intermolecular forces between solid and fluid can be represented by the inclusion of the surface free energy in the expression of the total free energy [31]. Based on the Cahn theory they proposed three kinds of polynomial boundary conditions: linear, quadratic, and cubic to predict the contact angle and density distribution around the wall and made comparisons. The results shown that these three types of boundary conditions have own particular advantages on specific cases. The cubic boundary scheme was applied in Lee and Liu's work on contact angle simulation and showed good accuracy [20]. Connington and Lee [22] then extended the model [20] to simulate the behavior of droplets on super hydrophobic surfaces with a new implementation of boundary conditions for the complex geometry and an addition of extra force

in 2013. The simulations reproduced the experimental contact angles well both in the Cassie and Wenzel states (on surfaces with different roughness), however, the transition between these states, which is a dynamic process, was not successfully modelled. Therefore, it can be concluded that the moving contact line phenomenon is not easy to reproduce by LB method.

In this paper, we aim to propose a mass conservative lattice Boltzmann model to simulate the two-phase flows with moving contact lines at high density ratio. The proposed model consists of a phase field lattice Boltzmann equation (LBE) for solving the conservative Allen-Cahn (A-C) equation, and a pressure evolution LBE for solving the incompressible Navier-Stokes equations. In addition, a modified wall boundary treatment scheme is developed to ensure the mass conservation. The wetting dynamics are treated by incorporating the cubic wall energy in the expression of the total free energy. A series of numerical experiments including equilibrium droplets on wetting surface, co-current flow and a droplet moving by gravity along inclined wetting surfaces are conducted with the proposed model and the results are compared with the analytical solutions and experimental results for validation.

The rest of the paper is organized as follows: The mass conservation LB model will be introduced in the Sec.2. In Sec.3 we will apply the model on several benchmarks for validation and then discuss the behaviors of the moving down droplets along inclined surfaces, and the paper is concluded in Sec. 4 with a brief summary.

2.METHOD

2.1 Discrete Boltzmann Equations for Incompressible Two-phase Fluids

The Navier-Stokes equation is usually adopted to describe the fluid dynamics, and it can be recovered by the particle distribution function $\boldsymbol{f}$ in lattice Boltzmann methods. The governing equation of $\boldsymbol{f}$, which is the discrete Boltzmann equations (DBE) describing the transportation of density and momentum of the incompressible two-phase fluids, is taken as

$$\left(\frac{\partial}{\partial t}+\boldsymbol{e}_\alpha\cdot\nabla\right)f_\alpha=-\frac{1}{\lambda}\left(f_\alpha-f_\alpha^{eq}\right)+\frac{1}{{c_s}^2}(\boldsymbol{e}_\alpha-\boldsymbol{u})\cdot\boldsymbol{F}\Gamma_a, \tag{1}$$

where f_α, $\boldsymbol{e}_\alpha$ are the particle distribution function and the velocity of particle in direction α, $\boldsymbol{u}$ is the macro velocity, c_s is the lattice sound speed and λ is the relaxation time, $\Gamma_a=\Gamma_a(\boldsymbol{u})=f_\alpha^{eq}/\rho$, and f_α^{eq} is the equilibrium distribution function which is defined by Eq. (2) [32]

$$f_\alpha^{eq}=\omega_\alpha\rho\left[1+\frac{\boldsymbol{e}_\alpha\cdot\boldsymbol{u}}{c_s^2}+\frac{(\boldsymbol{e}_\alpha\cdot\boldsymbol{u})^2}{2c_s^4}-\frac{(\boldsymbol{u}\cdot\boldsymbol{u})}{2c_s^2}\right], \tag{2}$$

where ω_α donates the weight factor.

The force terms $\boldsymbol{F}$ in Eq. (1) can have different forms. In this study we take the force scheme proposed by Lee and Liu [20]

$$\boldsymbol{F} = \nabla\rho c_s^2 - \nabla p + \mu\nabla\phi + \boldsymbol{F}_b, \tag{3}$$

in which ϕ is order parameter referring different phases, $\boldsymbol{F}_b$ is the body force and μ represents the chemical potential, which is a function of the order parameter ϕ

$$\mu = 4\beta(\phi-\phi_h)(\phi-\phi_l)\left(\phi-\frac{\phi_h+\phi_l}{2}\right)-\kappa\nabla^2 C, \tag{4}$$

where ϕ_h and ϕ_l indicate the different phases and are referred as 1 (liquid phase) and 0 (gas phase). κ and β are the parameters related to the surface tension σ and interface width W. This scheme can ensure that the computation of $\boldsymbol{F}$ in collision process is local.

Similar to using the h_α to recover Allen-Cahn equation, a new distribution function, g, is introduced here to describe the evolution of pressure p, which is defined as

$$g_\alpha = f_\alpha c_s^2 + \omega_\alpha\left(p-\rho c_s^2\right), \tag{5}$$

and the corresponding equilibrium distribution function of g is defined as

$$g_\alpha^{eq} = \omega_\alpha\left[p+\rho c_s^2\left(\frac{\boldsymbol{e}_\alpha\cdot\boldsymbol{u}}{c_s^2}+\frac{(\boldsymbol{e}_\alpha\cdot\boldsymbol{u})^2}{2c_s^4}-\frac{(\boldsymbol{u}\cdot\boldsymbol{u})}{2c_s^2}\right)\right]. \tag{6}$$

According to Eq. (1) the DBE for the new variable g_α is taken as

$$\left(\frac{\partial}{\partial t}+\boldsymbol{e}_\alpha\cdot\nabla\right)g_\alpha = -\frac{g_\alpha-g_\alpha^{eq}}{\lambda}+(\boldsymbol{e}_\alpha-\boldsymbol{u})\cdot[\nabla\rho c_s^2(\Gamma_a-\omega_\alpha)+(\boldsymbol{F}_b+\mu\nabla\phi)\Gamma_a]. \tag{7}$$

Noticing that $\rho = \rho_l+\phi(\rho_h-\rho_l)$, in which ρ_h and ρ_l represent the densities of liquid and gas phases. Accordingly we have

$$\nabla\rho = (\rho_h-\rho_l)\nabla\phi, \tag{8}$$

which can bring a great reduction of computation loads for $\nabla\rho$.

The DBE for g_α can also be split into collision and streaming processes. To simplify the calculation, the modified distribution functions $\overline{g}_\alpha$ as well as their equilibrium functions $\overline{g}_\alpha^{eq}$ are introduced as follows

$$\bar{g}_\alpha = g_\alpha + \frac{1}{2\tau}\left(g_\alpha - g_\alpha^{eq}\right) - \frac{\delta_t}{2}\left(\boldsymbol{e}_\alpha - \boldsymbol{u}\right)\cdot\left[\nabla\rho c_s^2\left(\Gamma_a - \omega_\alpha\right) + \left(\mu\nabla\phi + \boldsymbol{F}_b\right)\Gamma_a\right], \tag{9}$$

$$\bar{g}_\alpha^{eq} = g_\alpha^{eq} - \frac{\delta_t}{2}\left(\boldsymbol{e}_\alpha - \boldsymbol{u}\right)\cdot\left[\nabla\rho c_s^2\left(\Gamma_a - \omega_\alpha\right) + \left(\mu\nabla\phi + \boldsymbol{F}_b\right)\Gamma_a\right], \tag{10}$$

where τ is the dimensionless relaxation time which is defined as $\tau = \lambda / \delta_t$, and δ_t is the time step.

Finally the collision process can be expressed as followed

$$\tilde{g}_a\left(\boldsymbol{x},t\right) = \bar{g}_\alpha\left(\boldsymbol{x},t\right) - \frac{\left(\bar{g}_\alpha - \bar{g}_\alpha^{eq}\right)|_{(\boldsymbol{x},t)}}{\tau} + \delta_t\left(\boldsymbol{e}_\alpha - \boldsymbol{u}\right)\cdot\left[\nabla\rho c_s^2\left(\Gamma_a - \omega_\alpha\right) + \left(\mu\nabla\phi + \boldsymbol{F}_b\right)\Gamma_a\right]_{(\boldsymbol{x},t)}, \tag{11}$$

where $\tilde{g}_a\left(\boldsymbol{x},t\right)$ is the updated $\bar{g}_\alpha$ after the collision.

The streaming is then carried out under the perfect shift scheme

$$\bar{g}_\alpha\left(\boldsymbol{x} + \boldsymbol{e}_\alpha\delta_t, t + \delta_t\right) = \tilde{g}_a\left(\boldsymbol{x},t\right). \tag{12}$$

2.2 Discrete Boltzmann Equations (DBE) for the Allen-Cahn Equation

The Allen–Cahn equation is a phase field equation which describes the process of phase separation in multi-phase systems. The order parameter $\phi\left(\boldsymbol{x},t\right)$ is used in the phase field model to track the two-phase interface, which satisfies the following conservative Allen-Cahn equation

$$\frac{\partial\phi}{\partial t} + \nabla\cdot\phi\boldsymbol{u} = \nabla\cdot\left[M\left(\nabla\phi - \frac{1-4\left(\phi-\frac{\left(\phi_h+\phi_l\right)}{2}\right)^2}{W}\right)\boldsymbol{n}\right], \tag{13}$$

where ϕ_h and ϕ_l indicate the different phases and $\left(\phi_h + \phi_l\right)/2$ locates the interface in the impressible two-phase flows (ϕ_h, ϕ_l are referred as 1 and 0 in this study to represent the two phases). The parameters M, $\boldsymbol{u}$, W represent the mobility, macroscopic velocity and interface width respectively, and $\boldsymbol{n}$ is the normal vector to the interface, which is defined by

$$\boldsymbol{n} = \frac{\nabla\phi}{\left|\nabla\phi\right|}. \tag{14}$$

When the system reaches an equilibrium state, the equilibrium distribution of ϕ along the direction z normal to the interface is assumed as a hyperbolic tangent profile

$$\phi\left(\mathrm{z}\right) = \frac{\left(\phi_\mathrm{h} + \phi_\mathrm{l}\right)}{2} + \frac{\left(\phi_\mathrm{h} - \phi_\mathrm{l}\right)}{2}\tanh\left(\frac{2\mathrm{z}}{\mathrm{W}}\right). \tag{15}$$

A new function h_α, which is the distribution function of ϕ, is introduced for solving Eq. (13), and the LB equation of h_α is

$$\left(\frac{\partial}{\partial t}+\boldsymbol{e}_\alpha\cdot\nabla\right)h_\alpha=-\frac{h_\alpha-h_\alpha^{eq}}{\lambda}, \tag{16}$$

where λ is the relaxation time related to the phase-field parameters.

The equilibrium distribution function of h_α is

$$h_\alpha^{eq}=\phi\Gamma_a+B\omega_\alpha\boldsymbol{e}_\alpha\cdot\boldsymbol{n}, \tag{17}$$

where the term $B\omega_\alpha\boldsymbol{e}_\alpha\cdot\boldsymbol{n}$ accounts for anti-diffusion and in which

$$B=\frac{M}{c_s^{\,2}}\left[\frac{1-4\left(\phi-\frac{\left(\phi_h+\phi_l\right)}{2}\right)^2}{W}\right]. \tag{18}$$

Following the original lattice Boltzmann scheme, the distribution function h_α is going through the collision and streaming processes. In the collision process, h_α satisfies

$$\tilde{h}_a=h_\alpha-\frac{h_\alpha-h_\alpha^{eq}}{\tau_h}, \tag{19}$$

where τ_h is the dimensionless relaxation time and is related to the mobility by

$$\tau_h=0.5+\frac{M}{c_s^{\,2}\delta t}. \tag{20}$$

After the collision process, the streaming occurs under the perfect shift scheme as followed

$$h_\alpha\left(x+e_\alpha\delta_t,t+\delta_t\right)=\tilde{h}_a\left(x,t\right). \tag{21}$$

Then, the hydrodynamic parameters such as the average velocity and dynamic pressure can be calculated by taking the zeroth of the distribution function h_α as shown in Eq. (22)

$$\phi=\sum_\alpha h_\alpha. \tag{22}$$

After the streaming step, the hydrodynamic parameters such as the average velocity and the dynamic pressure can be calculated by taking the zeroth and first moments of the particle distribution

$$\boldsymbol{u}=\frac{1}{\rho}\left(\frac{1}{c_s^2}\sum_\alpha\boldsymbol{e}_\alpha\bar{g}_\alpha+\frac{\delta t}{2}\left(\mu\nabla\phi+\boldsymbol{F}_b\right)\right), \tag{23}$$

$$p = \sum_{\alpha} \overline{g}_{\alpha} + \frac{\delta t}{2} \boldsymbol{u} \cdot \nabla \rho c_s^2 . \tag{24}$$

2.3 Treatment of wetting wall boundary

The wetting wall boundary is treated from two respects: the "ordinary" boundary treatment and the wetting boundary treatment. The former is to obtain the distribution functions at the wall points and the latter is to properly reflect the wetting condition in the wall parameters.

Fig. 1 shows the lattice node configuration on a flat wall (D2Q9 scheme applied), where layer *N* is the boundary layer and x_b is the boundary point of layer *N*, f is the distribution function and i refers to the direction towards the fluid domain while $_{\bar{i}}$ points to the opposite direction (towards wall). The traditional bounce back scheme was widely adopted to the "ordinary" boundary treatment, in which the boundary points on layer *N* are not involved into collision process. However, according to our numerical experiments conducted in this study, the traditional bounce back scheme results to the mass unbalance problem, which may be attributed to the absence of boundary points in the collision process. Therefore, we proposed a modified bounce back scheme in which the boundary points (layer *N*) are involved the standard collision-streaming process as the points inside fluid field (layer *N*-1). The distribution functions towards the fluid domain of boundary points can be obtained as followed

$$f_i\left(\boldsymbol{x}_b, t+dt\right) = f_{\bar{i}}\left(\boldsymbol{x}_b, t+dt\right), \tag{20}$$

Then the order parameter ϕ_s at the wall boundary can be obtained by Eq. (18).

According to the phase-field theory, the free energy of the entire fluid system can be expressed as a function of ϕ

$$\Phi_b + \Phi_s = \int_V \left(E_0\left(C\right) + \frac{\kappa}{2}\left|\nabla\phi\right|^2 \right) dV + \int_S \left(\varphi_0 - \varphi_1\phi_s + \varphi_2\phi_s^{\,2} - \varphi_3\phi_s^{\,3} + \ldots \right) dS , \tag{21}$$

where E_0 is the bulk energy density and it usually takes the form as $E_0 = \beta C^2\left(C-1\right)^2$, κ is a constant related to the surface energy and β is a constant related to bulk energy. The chemical potential is defined as $\mu = \frac{\partial E_0}{\partial C} - \kappa\nabla^2\phi$.

Liu and Lee [31] made an assumption that the fluid behavior along the solid boundary is dominated by the interactions between the solid and liquid-gas interface, so the interactions between the solid and bulk fluids are not taken into consideration. The cubic boundary condition can be constructed based on this assumption and then the parameters in Eq. (21) can be chosen as: $\varphi_0 = \varphi_1$, $\varphi_2 = 1/2\varphi_w$, $\varphi_3 = 1/3\varphi_w$, where φ_w is a constant related to the dimensionless wetting potential *wp* as shown in Eq. (22)

$$wp = \varphi_w / \sqrt{2\kappa\beta}\,. \tag{22}$$

The cubic boundary condition for the order parameter ϕ_s at the wall is finally acquired by neglecting the terms higher than the third order in Φ_s and minimizing the total free energy $\Phi_b + \Phi_s$, which can be expressed as

$$\boldsymbol{n}\cdot\nabla\phi|_s = \left(\phi_s - \phi_s^{\,2}\right)\varphi_w / \kappa\,. \tag{23}$$

According to the Young's law, the wetting potential ω can be determined by the equilibrium contact angle θ^{eq}

$$\omega = -\cos\theta^{eq}\,. \tag{24}$$

Eq. (22), (23), (24) associate the gradient of order parameter $\nabla\phi$ and the contact angle θ^{eq}. The $\nabla\phi$ can be calculated with a given θ^{eq}, and then the chemical potential can be obtained by Eq. (4), and finally the macro parameters at the wall can be obtained by Eq. (18).

2.4 Calculation of Gradients

Different from the work done by Lee and Liu [20] in which a mixture of central difference and biased difference was taken for the calculation of the gradients, we adopted the central difference to obtain the gradients of the order parameter and the pressure, as defined by Eq. (31)

$$\nabla\phi|_x = \frac{1}{c_s^2\delta_t}\sum_{a\neq 0}\omega_\alpha \boldsymbol{e}_\alpha\left(\delta_t\boldsymbol{e}_\alpha\cdot\nabla\right)\phi|_x\,, \tag{25}$$

in which

$$\delta_t\boldsymbol{e}_\alpha\cdot\nabla^{CD}\phi|_x = \frac{1}{2}\left[\phi\left(\boldsymbol{x}+\boldsymbol{e}_\alpha\delta_t\right) - \phi\left(\boldsymbol{x}-\boldsymbol{e}_\alpha\delta_t\right)\right]. \tag{26}$$

The Eq. (14) can be discretized by using this finite difference (FD) scheme. For researcher who want to perform a parallel computation algorithm, Fakhari et al [24] provided a local method using central moments to discretize the Eq. (14). In this study we choose the finite difference scheme considering it was reported more accurate and stable [33].

3.RESULTS AND DISCUSSIONS

In this section we apply the model on two benchmark cases including equilibrium droplets on wetting surfaces and co-current flow. The results are compared with analytical solutions and experimental results. The behaviors of the water droplets moving by gravity along inclined

surfaces such as glass pane and steel plate are then simulated with this model, and the dynamics of moving contact line motion are captured and compared with experimental results.

We adopted the following two dimensionless parameters in analyzing simulation results, the density ratio as defined by Eq. (33) and the Cahn number as defined by Eq. (34)

$$\rho^* = \rho_H / \rho_L , \tag{27}$$

$$Cn = L_c / W , \tag{28}$$

where L_c refers the characteristic length and W is the interface width. Cn is often recommended to be greater than 10 to ensure the accuracy of simulations.

3.1Equilibrium droplet on wetting surfaces

In this case, a rectangle computational domain with a grid size of $NX \times NY$ is chosen. A two-dimensional liquid droplet with a radius of R is initially generated at the center of the wetting surface (as shown in Fig. 1a). The periodic boundaries are implemented at the left and right sides and the developed new wall boundary conditions are applied to the top and bottom boundaries. While the top surface has a fixed contact angle of $\theta^{eq} = 90°$, different contact angles ranging from $30°$ to $150°$ are assumed on the bottom surface.

The density ratio (the heavier over the lighter fluid, ρ^*) is taken as 1000 and $Cn = 20$. The other parameters are set as: $NX = 600, NY = 200, R = 80$. Fig 1 shows the equilibrium states of the droplet on wetting surfaces with contact angles of $\theta^{eq} = 30°, 60°, 90°, 120°$ and $150°$, in which the color represents the density while the red part and blue part are corresponding to the liquid droplet and the gas, respectively. Eq. (28) gives the theoretical relationship between θ^{eq} and wetting potential *wp*. The comparison between the simulated results and analytical solutions is presented in Fig. 2. The simulated equilibrium contact angles are measured by the geometric formula of droplet height and the length of contact line based on Fig 1 (b) to (f). It can be seen that the angles obtained by the present model agree well with the analytical ones. Furthermore, the droplet automatically achieved equilibrium state from initial state after a short period, which indicates that the current model is appropriate to handle the contact angle issue.

Due to the existence of gravity, the actual contact angle may differ from the theoretical ones. The testing-table shown in Fig. 3 is used to observe the actual contact angles between water and two surfaces with different materials. Fig. 4 compares the experimental and simulation results of different static contact angles while gravity exists, and the difference are $0.2°$ and $0.5°$, respectively. Considering the measuring error, the results by present model agree

well with the experiment. It is shown that the actual contact angle can be recovered accurately by our model, which indicates that the incorporation of the gravity works well.

3.1.1 Mass conservation

One of the most important features of our LB model is that it is mass conservative. The total mass of the system for droplet recovering process shown in Fig. 1b is checked to verify the mass conservation, and the results obtained from our model are compared with those of the model developed by Lee and Liu [20]. The total mass of the system M is normalized by the initial mass M_0, and its evolution process with dimensionless time is plotted in Fig. 5. It can be found that the system mass M gradually decreases with time in the method proposed in Ref. [20] while the total mass conserves ideally using our model.

3.1.2 Spurious currents

The spurious currents is a considerable issue in the multi-phase LB models. When the magnitude of spurious currents become as large as the characteristic velocities it would severely affected the reliability of the LB simulation results [34]. Fig. 7 shows the velocity field around a drop on a surface with contact angle 60 degree (the case of Fig 2 (c)). Vectors are magnified by $3X10^{11}$ at equilibrium state. It is indicated that the spurious currents have little influence on the results considering the magnitude compared to the characteristic velocity in our model.

3.2 Two-phase co-current flow in the infinite channel

In addition to the static case presented above, the performance of the model in simulating dynamic process is also tested. The two-phase co-current flow driven by an external force $\boldsymbol{F}$ in a channel is simulated. To examine the accuracy and stability of the present model, the symmetric co-current flow in the infinite channel is introduced here and the flow configuration is displayed in Fig. 6. The computational domain consists of a rectangle grids system $(NX \times NY)$, while the liquid phase occupies the areas in which $Y = -H1 \sim -H2$ and $Y = H1 \sim H2$, and the remaining area is occupied by the gas phase. Periodic boundaries are implemented at the left and right sides and the developed wall boundary conditions are applied to the top and bottom surfaces. The contact angles θ^{eq} of the top and bottom surfaces are set as $90°$. An external force in x direction, F_x, is exerted on the gas phase or liquid phase, respectively, which may result in different velocity distributions according to Ref. [35].

The density ratio is taken as 1000, i.e. $\rho^* = 1000$ in this case and $Cn = 10$. The other parameters are set as: $NX = 200, NY = 100, H1 = 25, H2 = 50$. Analytical solution for this type of flow can be

found in [35,36]. Fig. 7 and Fig. 8 show the velocity profiles of u_x for cases where F_x is applied on gas and liquid respectively, and the theoretical results are also presented. It can be seen that the velocity profiles obtained from the developed model agree well with analytical solutions.

3.3 Two-phase flow with moving contact line

To investigate the dynamics of two-phase flow with moving contact line, the behaviours of the water droplet moving by gravity along inclined wetting surfaces such as glass pane and steel plate are simulated using the model developed in this study. The computational domain consists of an inclined wall shown in Fig 9, where α is the angle of inclination. Similar to the case in 3.1, the boundaries in X directions are set as periodic boundaries, and the developed wall boundary conditions are applied to the surfaces in Y directions. The contact angle θ^{eq} is assigned to the inclined wall, which can be adjusted according to the real situations.

In this case $\rho^* = 775$ is taken, which represents the density ratio set of water and air, and the Cahn number $Cn = 30$ is taken to ensure the stability and accuracy. The grid system size is $Cn = 30$ 300X1000. The initial condition is shown in Fig 9: a droplet starts to move due to the gravity. The acceleration is set as g . The velocity profiles are set as follows

$$u_{x,liquid} = u_{x,gas} = 0, \tag{29}$$

$$u_{y,liquid} = u_{y,gas} = 0. \tag{30}$$

Experiments were also conducted on the test-table shown in Fig 3. A glass pane and a steel plate were used as the wall surface, while the working fluid is water in the test.

3.3.1 Advancing and receding contact angles

The contact angle hysteresis phenomenon is observed and discussed by many researchers [37,38] which focus on the wetting issue, and rather than static contact angles, they usually defined the contact angle hysteresis as the difference between θ_A and θ_R [39], where θ_A and θ_R represented the advancing (towards the heading) and receding (towards the backward) contact angles shown in Fig 10. The contact angle hysteresis may attribute to various factors such as surface roughness and the moving velocity. A water droplet of volume 20μL was put on the steel plate with an inclined angle of $60°$ to observe the phenomenon. Fig 10a shows the moving droplet and the contact angles captured at certain moment in the experiment. The measured θ_A and θ_R are around $75°$ and $40°$ respectively. This phenomenon was also recovered by using the current model as shown in Fig 10b. There is a little difference between the simulation and experimental results, which the θ_A and θ_R are about $77°$ and $45°$ in

former situation. This may result from the neglect of the surface roughness in our model. The comparison shown in Fig 10 indicates that the present model is capable to capture the advancing and receding contact angles in the droplet moving process.

3.3.2 Evolution of moving contact line

The glass pane is a hydrophilic surface with a static contact angle as low as $22.1°$. A water droplet of volume $20\mu L$ was put on the glass pane with an inclined angle of $40°$ in the experiment test. Evolution of the moving droplet along the glass pane is captured and shown from Fig 11a to Fig 11d, in which the left pictures are experiment results and right ones are outputs by our proposed model. It can be observed that the droplet moves at a nearly constant velocity after an acceleration at the beginning. The contact angles in Fig 11d, both advancing and receding contact angles, are near to $22.1°$ while the former is a little larger and the latter smaller, which indicates the contact angle hysteresis exists. The phenomenon can also be observed in the simulation outputs, which agrees well with the experimental results. By comparing the experiment and simulation results in Fig 11 we can conclude that the moving contact line can be recovered accurately by the model developed in this study.

3.3.3 Computational effort

The falling droplet simulations are carried out on a computer with CPU i7-3930K and 16 GB RAM. The C++ compiler is the MSVC on windows platform. The computing time for the case in which droplet falls half length of the wall is 403 mins.

4 Conclusion

This paper presents a conservative lattice Boltzmann model to simulate the two-phase flows with moving contact line at high density ratio. The proposed model consists of a phase field lattice Boltzmann equation for solving the conservative Allen-Cahn equation, and a pressure evolution LBE for solving the incompressible Navier-Stokes equations. A modified wall boundary treatment scheme is developed to ensure the mass conservation. In addition, the wetting dynamics are treated by incorporating the cubic wall energy in the expression of the total free energy. The proposed model is featured with mass conservation property, proper treatment of wetting boundary and high density ratio. Numerical tests including equilibrium droplets on wetting surface, co-current flow and a droplet moving by gravity along inclined wetting surfaces are conducted with our proposed model. The simulation results agree well with analytical solutions and experimental results. The mass conservation is checked and confirmed, the wetting surface is accurately modelled and the density ratio is up to 1000 in the tests. Results show that the proposed model can successfully recover the moving contact line process, making it applicable to the study of moving contact line problem and further relevant applications.

Acknowledgement

The research work presented in this paper is financially supported by a research grant (4-BCAR) in the Hong Kong Polytechnic University and Postdoctoral Fellowships Scheme of the Hong Kong Polytechnic University (1-YW1D).

References

[1]. Chowdhury I, Prasher R, Lofgreen K, et al. On-chip cooling by superlattice-based thin-film thermoelectrics[J]. Nature nanotechnology, 2009, 4(4): 235.

[2]. Lu T, Xiao F. Lattice Boltzmann Simulation of Falling Film Flow under Low Reynolds Number[J]. Heat Transfer Engineering, 2017: 1-12.

[3]. Cox R G. The dynamics of the spreading of liquids on a solid surface. Part 1. Viscous flow[J]. Journal of Fluid Mechanics, 1986, 168: 169-194.

[4]. Cox R G. The dynamics of the spreading of liquids on a solid surface. Part 2. Surfactants[J]. Journal of Fluid mechanics, 1986, 168: 195-220.

[5]. Li, Q., Luo, K.H., Kang, Q.J., He, Y.L., Chen, Q., and Liu, Q., Lattice Boltzmann Methods for Multiphase Flow and Phase-Change Heat Transfer, Progress in Energy and Combustion Science, vol. 52, pp. 62-105, 2016.

[6]. Rothman D H, Keller J M. Immiscible cellular-automaton fluids[J]. Journal of Statistical Physics, 1988, 52(3): 1119-1127.

[7]. Shan X, Chen H. Lattice Boltzmann model for simulating flows with multiple phases and components[J]. Physical Review E, 1993, 47(3): 1815.

[8]. M.R. Swift, W.R. Osborn, J.M. Yeomans, Lattice Boltzmann simulation of nonideal fluids, Phys. Rev. Lett. 75 (1995) 830–833.

[9]. He X, Chen S, Zhang R. A lattice Boltzmann scheme for incompressible multiphase flow and its application in simulation of Rayleigh–Taylor instability[J]. Journal of Computational Physics, 1999, 152(2): 642-663.

[10]. Lee T, Liu L. Lattice Boltzmann simulations of micron-scale drop impact on dry surfaces[J]. Journal of Computational Physics, 2010, 229(20): 8045-8063.

[11]. Liang H, Chai Z H, Shi B C, et al. Phase-field-based lattice Boltzmann model for axisymmetric multiphase flows[J]. Physical Review E, 2014, 90(6): 063311.

[12]. Connington K, Lee T. Lattice Boltzmann simulations of forced wetting transitions of drops on superhydrophobic surfaces[J]. Journal of Computational Physics, 2013, 250: 601-615.

[13]. Zheng L, Lee T, Guo Z, et al. Shrinkage of bubbles and drops in the lattice Boltzmann equation method for nonideal gases[J]. Physical Review E, 2014, 89(3): 033302.

[14]. Fakhari A, Geier M, Lee T. A mass-conserving lattice Boltzmann method with dynamic grid refinement for immiscible two-phase flows[J]. Journal of Computational Physics, 2016, 315: 434-457.

[15]. Liang H, Xu J, Chen J, et al. Phase-field-based lattice Boltzmann modeling of large-density-ratio two-phase flows[J]. arXiv preprint arXiv:1710.09541, 2017.

[16]. Yan Y Y, Zu Y Q. A lattice Boltzmann method for incompressible two-phase flows on partial wetting surface with large density ratio[J]. Journal of Computational Physics, 2007, 227(1): 763-775.

[17]. Liu L, Lee T. Wall free energy based polynomial boundary conditions for non-ideal gas lattice Boltzmann equation[J]. International Journal of Modern Physics C, 2009, 20(11): 1749-1768.

[18]. Qian Y H. Simulating thermohydrodynamics with lattice BGK models[J]. Journal of Scientific Computing, 1993, 8(3): 231-242.

[19]. Geier M, Fakhari A, Lee T. Conservative phase-field lattice Boltzmann model for interface tracking equation[J]. Physical Review E, 2015, 91(6): 063309.

[20]. Huang H, Huang J J, Lu X Y, et al. On simulations of high-density ratio flows using color-gradient multiphase lattice Boltzmann models[J]. International Journal of Modern Physics C, 2013, 24(04): 1350021.

[21]. Huang H, Lu X. Relative permeabilities and coupling effects in steady-state gas-liquid flow in porous media: A lattice Boltzmann study[J]. Physics of Fluids, 2009, 21(9): 092104.

[22]. Chatain D. Experimental study of wetting hysteresis on surfaces with controlled geometrical and/or chemical defects[J]. Acta metallurgica et materialia, 1995, 43(4): 1505-1515.

[23]. Soolaman D M, Yu H Z. Water microdroplets on molecularly tailored surfaces: correlation between wetting hysteresis and evaporation mode switching[J]. The Journal of Physical Chemistry B, 2005, 109(38): 17967-17973.

[24]. Kabov O A, Zaitsev D V. The effect of wetting hysteresis on drop spreading under

gravity[C]//Doklady Physics. Springer US, 2013, 58(7): 292-295.

Figure Captions

Figure 1 Equilibrium state of droplets on surfaces with different contact angles. a: initial state, b: 30º, c: 60º, d: 90º, e: 120º, f: 150º.

Figure 2 The comparison between the equilibrium contact angles between simulation results and analytical data.

Figure 3 Test-table for testing the static and dynamic contact angles.

Figure 4 Comparison of the experimental and simulation results on actual contact angles. a,c: experiment, b,d: simulation.

Figure 5 Variation of the mass of the system versus time for the droplet recovering process in present model and Lee and Liu's model [10].

Figure 6 The configuration of two-phase co-current flow in the infinite channel.

Figure 7 Velocity profiles of the co-current flows with F_x applied on the gas

Figure 8 Velocity profiles of the co-current flows with F_x applied on the liquid

Figure 9 Initial state of the moving water droplet.

Figure 10 The experimental and simulation results of advancing and receding contact angles on inclined steel plate. a: experiment; b: simulation.

Figure 11 Evolution of moving droplet on inclined glass pane (Left: experiment results, Right: simulation results).

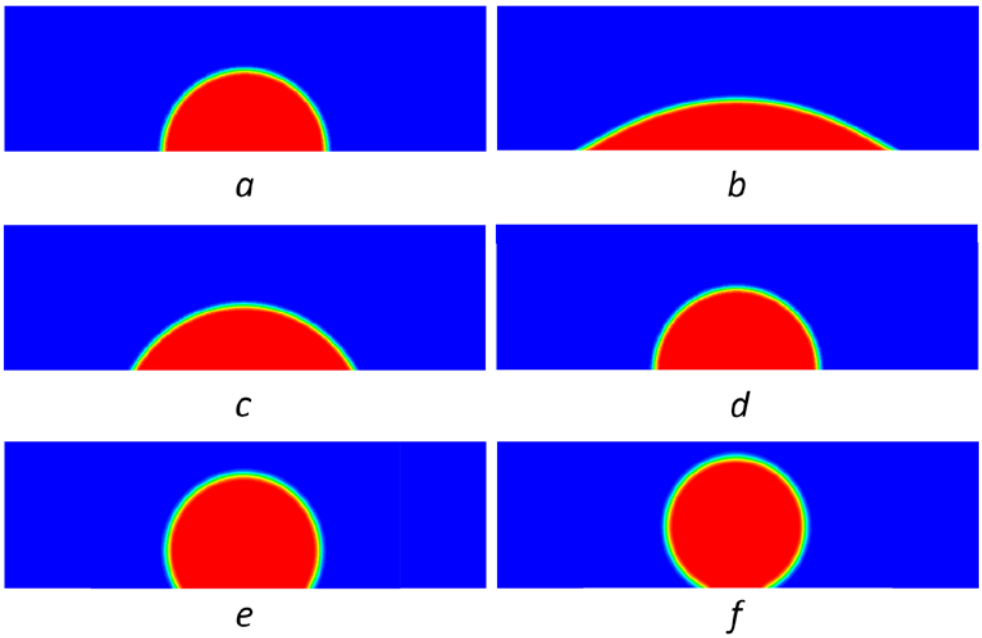

Figure 1 Equilibrium state of droplets on surfaces with different contact angles. *a*: initial state, *b*: 30º, *c*: 60º, *d*: 90º, *e*: 120º, *f*: 150º.

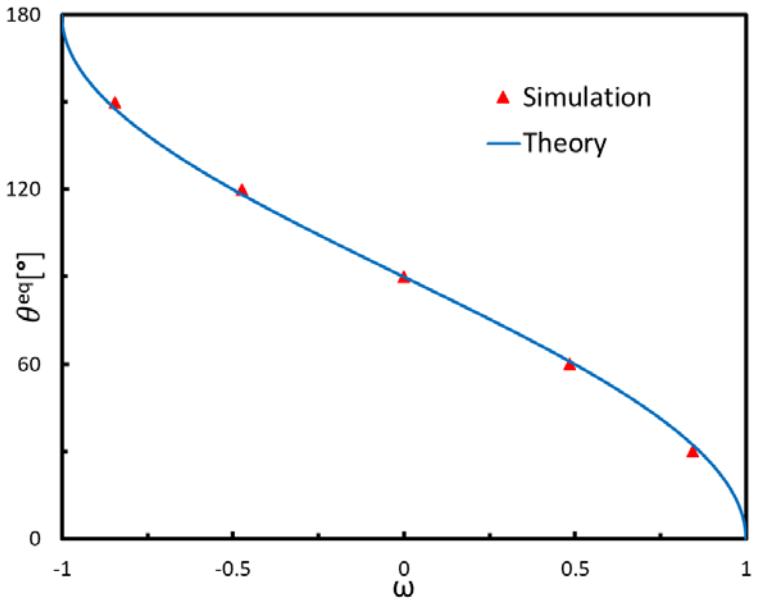

Figure 2 The comparison between the equilibrium contact angles between simulation results and analytical data.

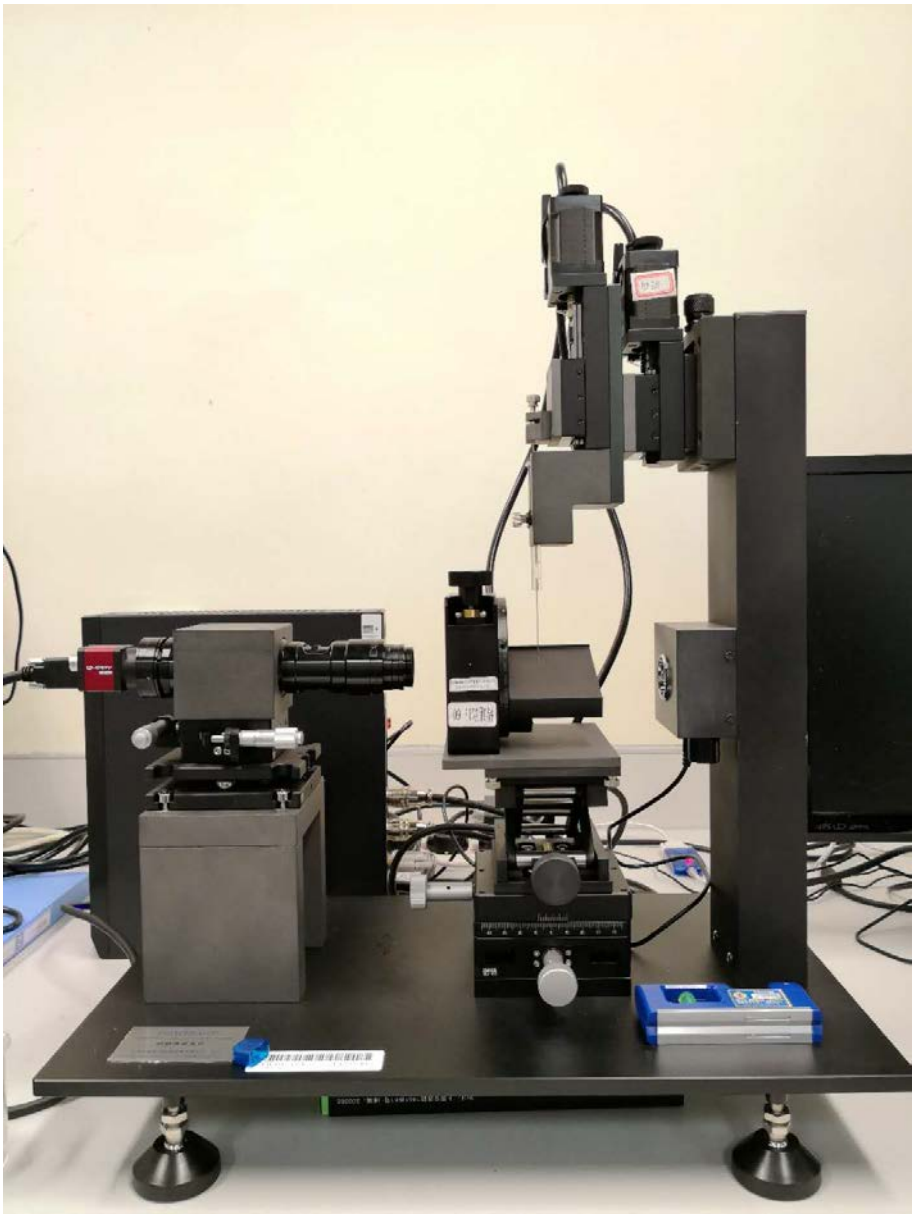

Figure 3 Test-table for testing the static and dynamic contact angles.

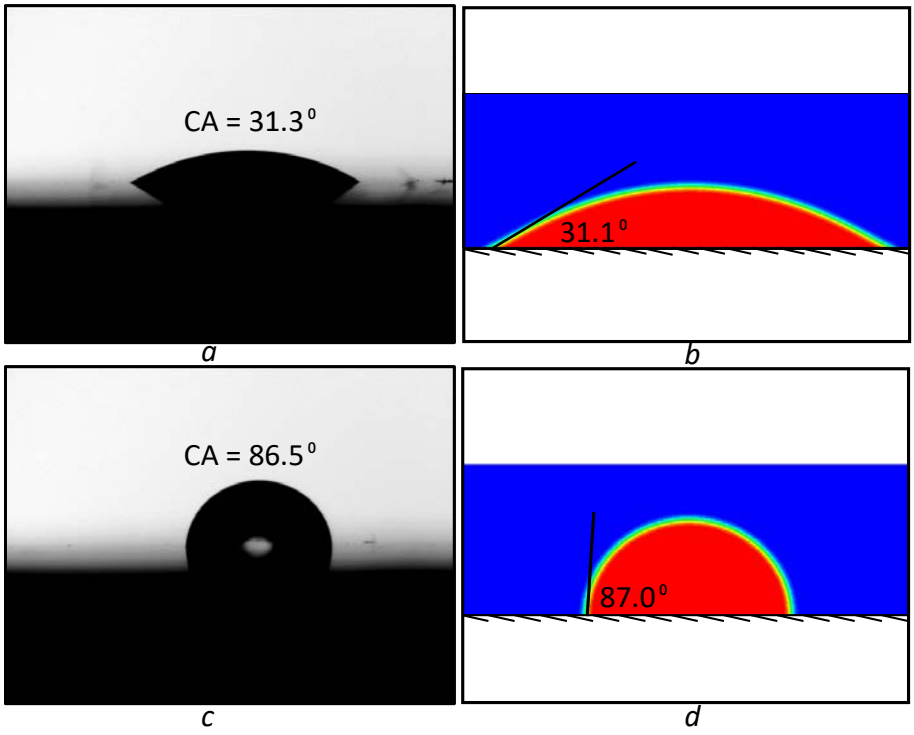

Figure 4 Comparison of the experimental and simulation results on actual contact angles. *a*,*c*: experiment, *b*,*d*: simulation.

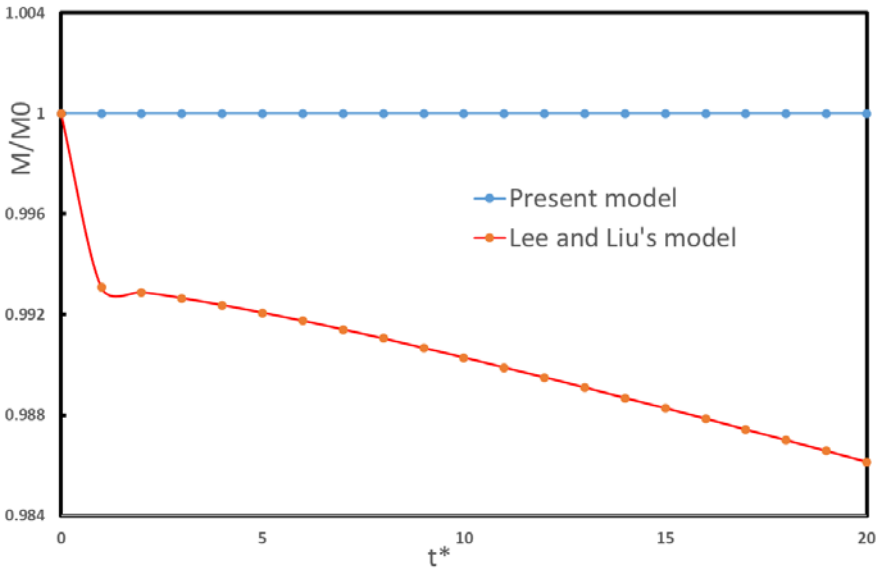

Figure 5 Variation of the mass of the system versus time for the droplet recovering process in present model and Lee and Liu's model [10].

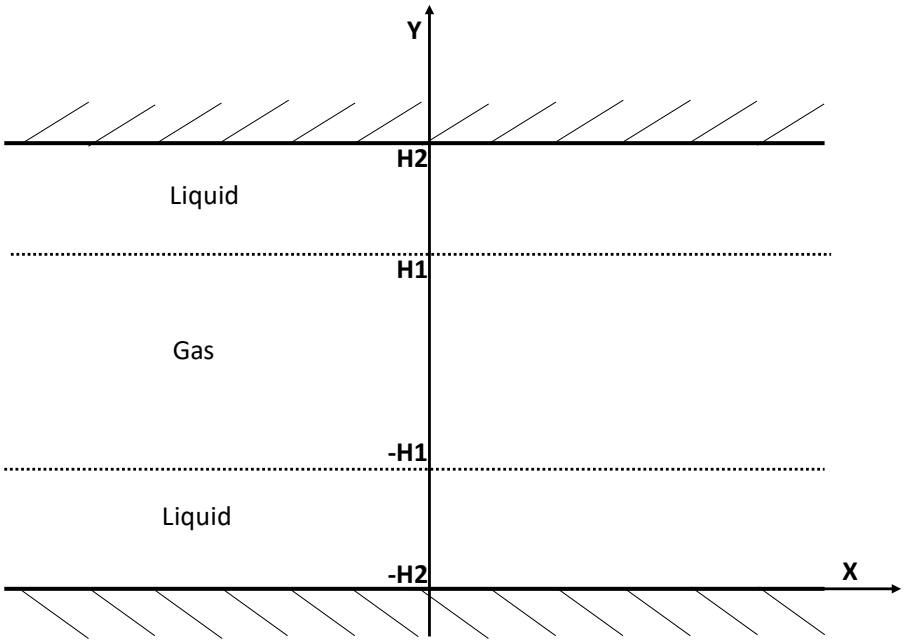

Figure 6 The configuration of two-phase co-current flow in the infinite channel.

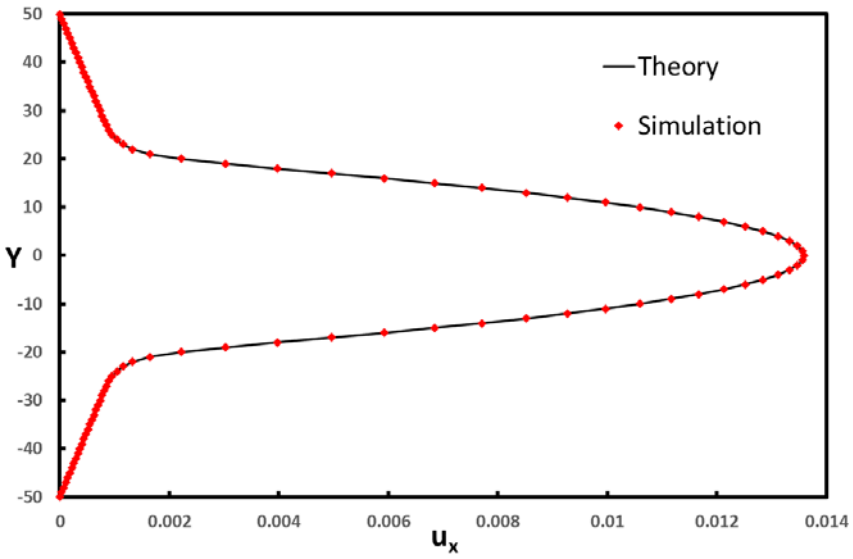

Figure 7 Velocity profiles of the co-current flows with F_x applied on the gas.

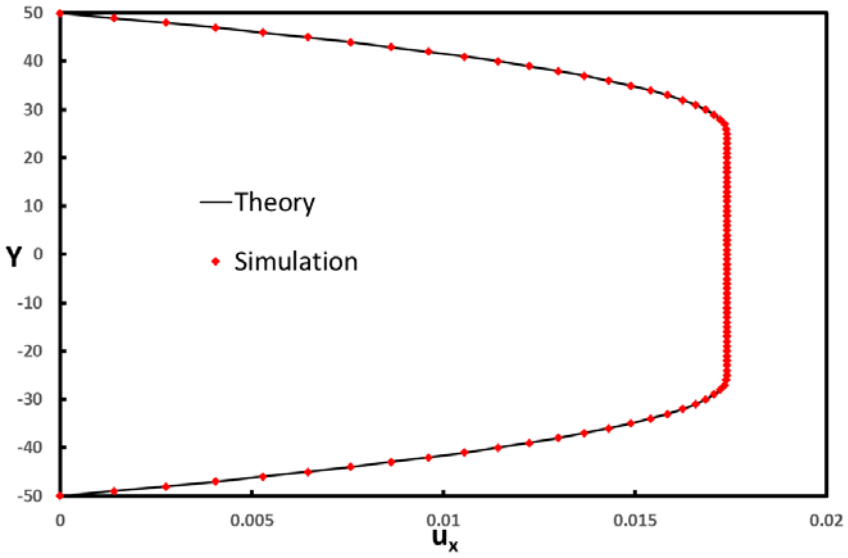

Figure 8 Velocity profiles of the co-current flows with F_x applied on the liquid.

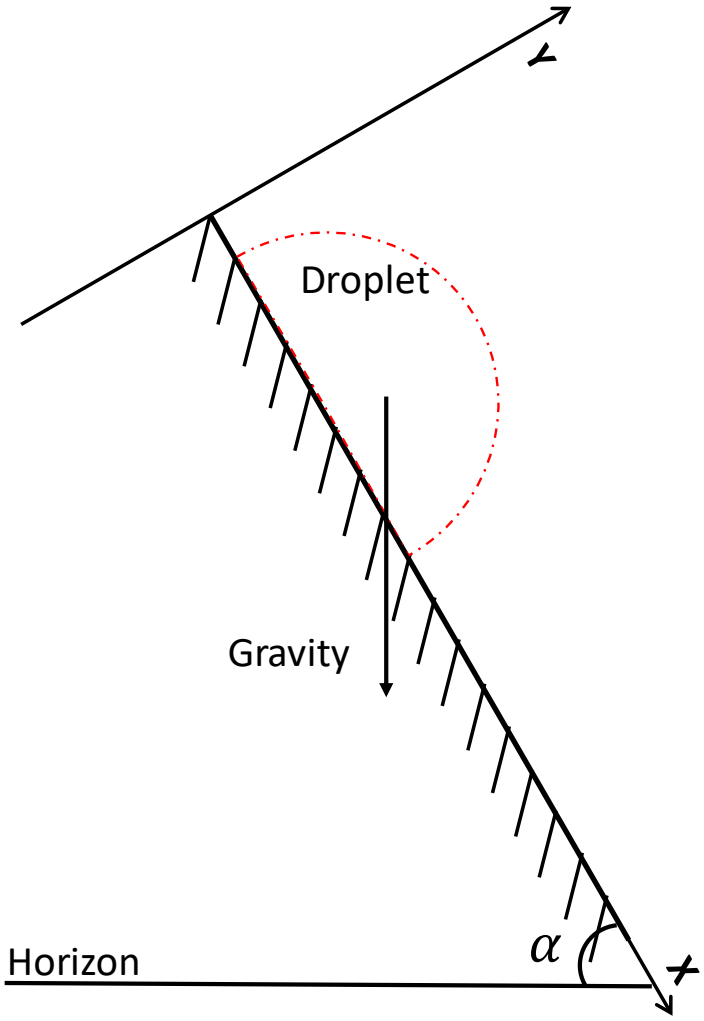

Figure 9 Initial state of the moving water droplet.

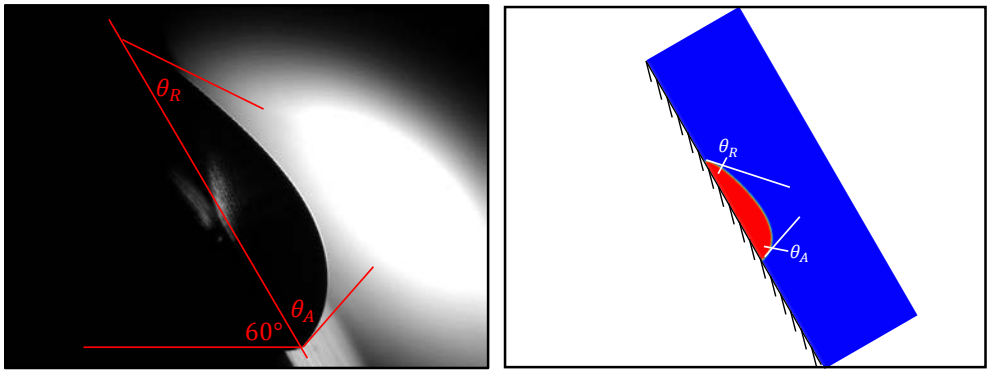

Figure 10 The experimental and simulation results of advancing and receding contact angles on inclined steel plate. *a*: experiment; *b*: simulation.

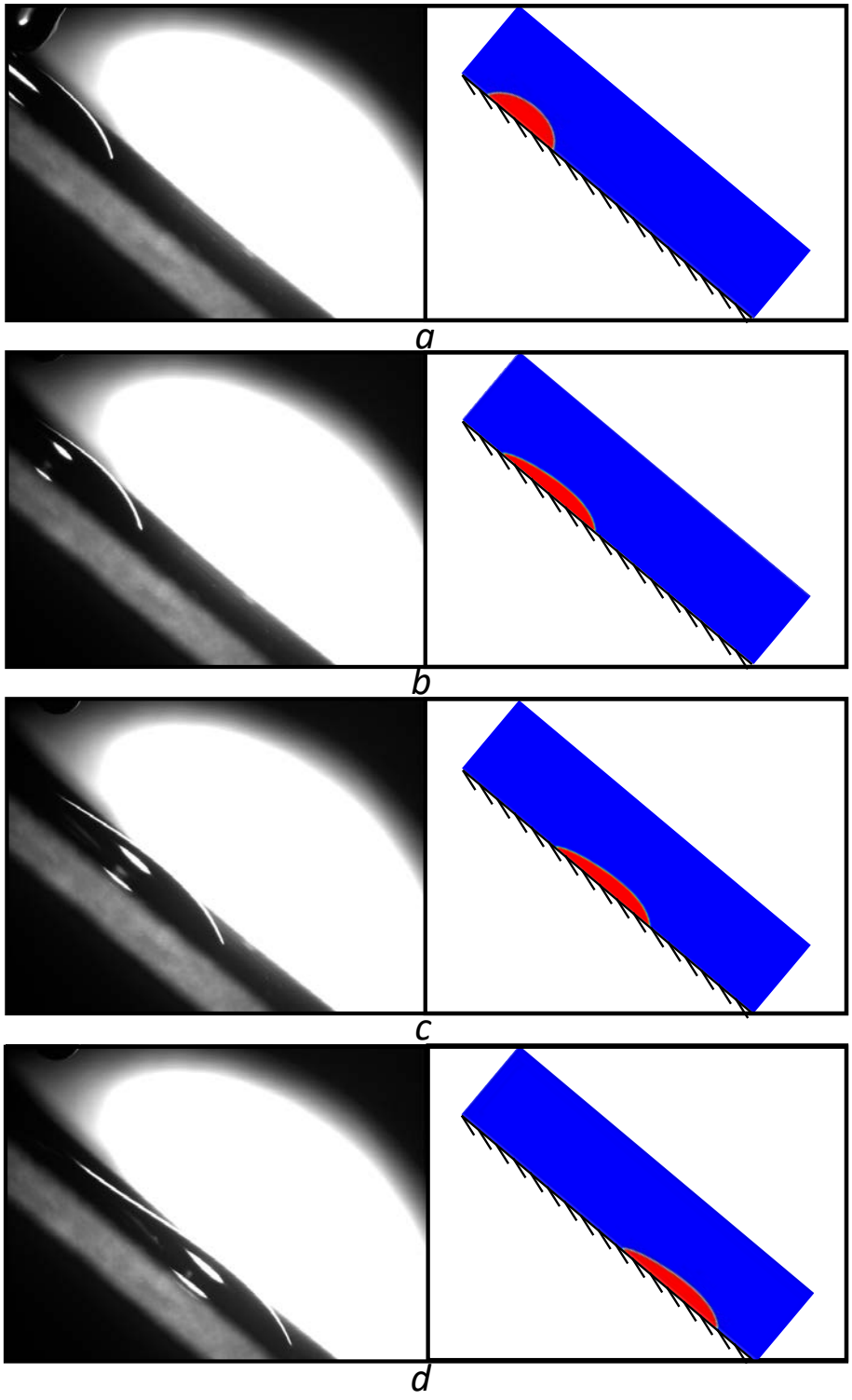

Figure 11 Evolution of moving droplet on inclined glass pane (*Left*: experiment results, *Right*: simulation results).